Development and testing of a 3D seismic velocity model of the Po Plain sedimentary basin, Italy.

Irene Molinari[1], Andrea Argnani[2], Andrea Morelli[3], and Piero Basini* [4]

[1]Istituto Nazionale di Geofisica e Vulcanologia - Sezione di Sismologia e Tettonofisica, Roma, Italy.

[2] Istituto di Scienze Marine - Consiglio Nazionale delle Ricerche, Bologna, Italy.

[3]Istituto Nazionale di Geofisica e Vulcanologia - Sezione di Bologna, Bologna, Italy.

[4]University of Toronto, Department of Physics, Toronto, Canada.

November 13, 2014

Abstract

We built a 3D seismic model of the Po Plain and neighboring regions of northern Italy, covering altogether an area about 600 km by 300 km with an approximately 1-km spaced grid. We started by collecting an extensive and diverse set of geological and geophysical data, including seismic reflection and refraction profiles, borehole logs, and available geological information. Major geological boundaries and discontinuities have thus been identified and mapped into the model. We used kriging to interpolate the geographically sparse information into continuous surfaces delimiting geological bodies with laterally-varying thickness. Seismic wave properties have been assigned to each unit using a rule-based system and v_P, v_S, and ρ derived from other studies. Sedimentary strata — although with varying levels of compaction and hence material properties — may locally reach a thickness of 15 km, and give rise to significant effects in seismic wave propagation. We have used our new model to compute the seismic

*now at Total SA, Exploration Technologies CSTJF, Avenue Larribau, 64018 Pau cedex, France

response for two recent earthquakes, to test its performance. Results show that the 3D model reproduces the large amplitude and the long duration of shaking seen in the observed waveforms recorded on sediments, while paths outside the basin may be well fit by more homogeneous (1D) hard rock structure. We conclude that the new model is suited for simulation of wave propagation, mostly for $T > 3s$, and may serve well as a constraint for earthquake location and further improvements via body or surface wave inversion.

Introduction

The Po Plain (northern Italy) hosts a wide sedimentary basin, where a thick Plio-Quaternary sedimentary sequence (up to 8 km thick) covers the foreland of the Alps and the fold-and-thrust belt of the Northern Apennines, shaped by the convergence of the African and European plates (e.g. Kligfield, 1979; Patacca et al., 1992). The foredeep sediments buried below the Po Plain are mainly of Pliocene-Pleistocene age, and show a remarkable south-westward thickening (e.g. Pieri and Groppi, 1981). These sediments fill the last basin in a system of north-eastward migrating foredeep basins that originated during the evolution of the Northern Apennines (Argnani and Ricci Lucchi, 2001). Present convergence rates amount to few mm per year (Devoti et al., 2011), and are responsible for some ongoing tectonic activity that manifests itself on the anticlines that lie buried under the plain. The low-strain rate tectonic activity causes infrequent, moderate-magnitude, earthquakes. Although being only characterised by a relatively moderate seismic hazard level, when compared to other areas in Italy — magnitude estimates for historical events hardly reach 6 — this region was hit severely by the 2012 earthquake sequence (Meletti et al., 2012), that included two $M \sim 6$ shocks due to reverse faulting mechanisms (Scognamiglio et al., 2012; Pondrelli et al., 2012), located on the blind thrusts of the western Ferrara arc (e.g. Burrato et al., 2012). During these events, the maximum recorded peak-ground accelerations have reached $0.3g$ at soft soil sites (Luzi et al., 2013), due to local amplification — not a very high value in absolute terms, but strong enough to make a significant societal impact. This area is in fact the economic center of Italy, and is characterized by large exposure because of the extensive presence of industry and highly populated urban centres.

It has been known for a long time that sedimentary basins significantly amplify ground motion (Anderson et al., 1986), because of the association of softer sedimentary units inside enclosing harder rocks, that amplify and trap energy. Relations have been proposed between ground motion and basin depth in specific seismic period bands (e.g. Hruby and Beresnev, 2003; Denolle et al., 2014). Sedimentary basins have shown to amplify specific frequencies. Besides, 3D geological structures can focus or de-focus seismic energy, and local soil conditions may further produce significant site effects. These effects result in significant variation of ground motion even on small length scales. Numerical earthquake simulations have been able to model such effects. Some notable examples worldwide include the Los Angeles basin (Olsen, 2000; Komatitsch et al., 2004),the San Francisco Bay area (Aagaard et al., 2008), the Kanto basin (Koketsu and Kikuchi, 2000; Dhakal and Yamanaka, 2013), the Osaka basin (Kagawa et al., 2004) and the Grenoble basin (Stupazzini et al., 2009; Chaljub et al., 2010). The Po Plain region is another such case, as it has been shown that ground motion prediction equations in general significantly underestimate seismic shaking above the basin (Bragato et al., 2011; Massa et al., 2012) and geographical variations are important. Massa et al. (2012) showed that the empirical models designed for the area provide a systematic underestimation of the recorded ground motion by a factor of 2 or larger, in particular for stations located on the basin borders. As possible causes, the authors suggested site amplification phenomena that also affect the longer periods ($T > 1s$). Luzi et al. (2013), after analysing the 2012 seismic sequence records, concluded that ground motion prediction equations for the Po plain area do not perform well, especially in the longer period range ($T > 1s$). These studies point out the fundamental role of the basin structure in amplifying the ground motion: deterministic modeling can help to better understand and estimate the characteristics of ground motion in this environment.

Detailed knowledge of three-dimensional crustal structure, especially at shallow depth, is a key element in understanding seismic wave propagation in any geologically complex region. Studies of seismic ground motion in sedimentary basins therefore follow efforts in building detailed 3D basin models from seismic and geological datasets (e.g. Magistrale et al., 2000; Süss and Shaw, 2003). Best known studies aimed at simulating long period ground motion are focussed in key areas characterized by the presence of deep sedimentary basins, high seismic hazard and high population density, such as the Los Angeles basin (e.g Magistrale et al., 1996; Süss and Shaw, 2003), the Santa Rosa basin (McPhee et al., 2007), the Osaka basin (Kagawa et al., 2004), the Adapazary-Turkey basin (Goto et al., 2005), and Alpine valleys (Roten et al., 2008). A key quality of a 3D model to be used for high frequency seismic ground motion simulations is to have adequate resolution of fine geological structures — ideally, a few hundred meters or less are desired. However, the sparsity of available information, confronted with the expected rapid spatial variability of the geological structure, makes the incorporation of geotechnical constraints into large 3D models problematic. Recent examples include the studies by Taborda and Bielak (2014) on the Los Angeles region, and by Flinchum et al. (2014) on the Las Vegas area.

In northern Italy, some regional-scale studies provided 3D images of the seismic structure of the crust and uppermost mantle. They include receiver function analyses — that mainly target Moho depth and v_P/v_S ratio (e.g. Piana Agostinetti and Amato, 2009; Spada et al., 2013) — and travel time and surface wave dispersion studies that represent either v_P or v_S volumetric variations in 3D (e.g. Di Stefano et al., 2009; Gualtieri et al., 2014; Stehly et al., 2009). Because of the need to impose smoothing conditions on the solution due to the sparsity of data coverage, tomographic models render geographical variations of structure with varying detail, but in general they fail to resolve the crustal layering and to represent the sharp discontinuities and impedance contrasts, that are very critical for wave reverberations and amplitude variations. The situation is specifically quite critical in the Po Plain region, where the seismic station distribution is sparse, and local seismicity is low. However, extensive high-resolution information is available in the form of seismic reflection profiles, borehole data and geological mapping (e.g. Cassano et al., 1986; Fantoni and Franciosi, 2010b; Bigi et al., 1990). Such studies add critical detail on interfaces, that are very consequential for local-scale seismic wave propagation.

In this contribution, we describe a high-resolution, 3D, crustal model that honors information derived from seismic exploration, and that can be used to model seismic wave propagation in the Po Plain region. In the following, we first describe the data that we used and the method we followed. We then describe the ensuing model, and finally we show results of a preliminary validation test done by modeling recorded seismograms from two recent events.

Dataset and method

We collected seismic reflection profiles, geological maps and borehole data relating to the Po Plain, that have mainly been obtained in the 1970's and the 1980's for hydrocarbon exploration (Figure 1). We used these data to constrain the 3D geometry of the model discontinuities (Figure 2), and to provide specific velocity-depth profiles inside each formation.

From the analysis of interpreted geophysical data we identified the major material discontinuities associated with lithological changes. We distinguished several geological units, that are described in the literature and that, because of their characteristics, are likely to have significant effects on seismic wave propagation. These units are also relevant from a geological, tectonic and seismogenetic point of view. For these units we gathered information on lithological properties and depth of their interfaces. A schematic stratigraphy column is shown in Figure 3a. At the top we defined a unit described as "loose sediments", that corresponds to the recent sandy and clay alluvial deposits of middle Pleistocene to recent age. Its base can be followed throughout the Po Plain thanks to water wells and shallow geophysical prospecting. The underlying unit is composed of the remaining Quaternary sediments, where marine clay and sand, with minor conglomerates, are dominant. The base of the Quaternary sediments is constrained by exploration wells and commercial seismic profiles. A Pliocene unit represented by claystone, marlstone, and sandstone is present below the Quaternary unit. The Pliocene sediments were mostly deposited during the formation of the arcuate thrust front that is buried under the Po Plain, and represent the Apennines foredeep basin fill. An Oligocene-Miocene unit, which is mostly expressed in northern Lombardy (western part of the Po Plain), consists of sandstones, claystones, and conglomerates. The sediments of this unit were deposited during the thrusting of the Southern Alpine front, and represent the retro-wedge foredeep basin of the Alps (Fantoni et al., 2004; Fantoni and Franciosi, 2010a). A unit with limited thickness is present between the base of the Oligocene-Miocene unit and the top of the Mesozoic unit. This unit, that is approximately of Paleocene-Eocene age, is characterised by stratified marlstones and limestones, with minor sandstones and clays. The calcium carbonate content increases remarkably with respect to the overlying siliciclastic sediments, causing an increase of seismic velocity. This unit records the initial Alpine mountain building, with limited clastic sediments derived from the growing orogen and deposited in a distal environment (Bortolotti et al., 1970). The Mesozoic unit is composed of stratified-to-massive limestones and dolomites, deposited in both shallow platform and basinal environments, and records the evolution of the Tethian passive margin (e.g. Masetti et al., 2010). From the mechanical point of view it can be considered the top of the seismogenic zone beneath the Po Plain. In several instances, the stratigraphy of exploration wells, obtained from the archives of the Italian Ministry of Energy (ViDEPI project), was used to check the extrapolated interfaces of the sedimentary units. In addition to the units described above, we also added the top of the units that are loosely described as ”magnetic basement”, and the base of the crust (Moho). The ”magnetic basement” is poorly characterised because of the limited sampling of pre-Triassic rocks, and of a large variability in magnetic susceptibility of Permian units. Given the limited data available, the magnetic basement can be taken as composed of slightly metamorphosed siliciclastic rocks (Permian Verrucano), and their metamorphic basement (Cassano et al., 1986; Speranza and Chiappini, 2002).

[Figure 1 about here.]

The data were gathered from many sources, summarising more than two decades of work (Figure 1). Pieri and Groppi (1981) and Cassano et al. (1986) interpreted seismic profiles shot in the 1970’s and 1980’s, together with gravimetric, magnetometric, borehole and surface geology data, and they translated them into depths of the main geological horizons, such as the lower boundaries of Quaternary, Pliocene, Paleogene and Mesozoic units. Cassano et al. (1986) also compiled a map of the top of the magnetic basement, identifying the top of the lithological or structural elements capable of producing magnetic signal — see also Speranza and Chiappini (2002) — that, as a first approximation, may represent the base of the Tethian sedimentary succession (Masetti et al., 2010). More recently, Fantoni and Franciosi (2010b) reconstructed a map of the thickness of the Messinian-Pleistocene (Apennine) and of the older Eocene-Messinian (Neoalpine) foredeep basin sediment. The contour lines describing the base of the Pliocene-Quaternary sequence are available in the *Structural Model of Italy* (Ogniben et al., 1975; Bigi et al., 1990). Additional efforts to refine and redraw the base of the Pliocene unit have been made by the Geological Service of the Emilia Romagna Region (RER and ENI-Agip, 1998) by elaborating and modifying the map by Bigi et al. (1990). Casero et al. (1990), on the basis of seismic profiles, boreholes, and surface data, presented a map of the top of the Mesozoic unit for the area encompassing the eastern part of the basin and the northern Adriatic. A map of the contour lines describing the top of Mesozoic rocks beneath North-Eastern Italy (Friuli-Venezia Giulia region) was presented by Nicolich et al. (2004). Work on confidential data sets of seismic profiles and boreholes, made available to us by ENI-AGIP, has allowed us to reconstruct the shape of the top of the carbonate unit beneath a large part of the Po Plain (R. Fantoni, personal communication). The thickness of unconsolidated sediments was obtained using the base of the porous and permeable deposits, mapped in detail by geological services of regions Emilia Romagna and Lombardia (RER and ENI-Agip, 1998; Carcano and Piccin, 2002). Crustal-scale seismic experiments, such as the Italian CROP program (Scrocca et al., 2003) and TRANSALP (Gebrande et al., 2006, and references therein), imaged the crustal structure of sectors of the Alps, Apennines and of the Adriatic and Tyrrhenian region. Finally, the Moho depth that we used was taken from the EPcrust reference model (Molinari and Morelli, 2011) that, in this area, consists of integration of results from Stehly et al. (2009) and Piana Agostinetti and Amato (2009). The free surface topography is from the SRTM 90-m Digital Elevation Data (Jarvis et al., 2008). Spatially, the geographical regions covered by each dataset are shown in Figure 1 and ranges from 44° to 46.5° N and from 7° to 14° E.

The 3D shape of each geological unit was obtained by merging all the retrieved information about the depth of each interface. Data in the form of analogue maps (such as for the Mesozoic, Oligo-Miocene and the magnetic basement) were geo-referenced and digitized with a GIS software, before being resampled into our working geographical resolution of $0.01° \times 0.01°$ degrees. In other cases, such as for the base of the Pliocene and the bottom of loose sediments, digital maps were available, and were just imported into our working framework.

We used the ordinary kriging estimation procedure as an interpolation scheme (i.e. Molinari et al., 2012). The ordinary kriging geostatistics allows us to characterize an unknown regionalized variable (a spatially-continuous, random function with some geographical distribution) from the samples in a neighbourhood of any unsampled location (i.e. Davis, 2002). We applied this method to model the surfaces marking the bottom of Quaternary and the top of Mesozoic. For some units (Figure 1), for each grid point we had more than one estimate available — this mainly was the case for Mesozoic. In fact, we collected three maps, partly overlapping, of the top of the Mesozoic discontinuity. To merge them, we applied a weighting scheme similar to Molinari and Morelli (2011) on the basis of date of publication, original resolution, number of data sets and method used, to represent a relative scale of reliability. In particular we assigned weights of 1 to the map newly drawn using the ENI-AGIP data (R. Fantoni, pers. comm.); 0.5 to the map by Casero et al. (1990); and 1 to the map by Nicolich et al. (2004).

Very little information on seismic properties (v_P, v_S) and density of the various geological units in the Po Plain are available from seismic prospection studies. Other published work describes P-wave velocity as a function of depth (first 5-8 km) and geologic time for a variety of relevant geological units, but for other areas. Brocher (2008) reported relations for Holocene and Plio-Quaternary, Tertiary and Mesozoic lithologies for California rocks. Faust (1951) measured P-wave velocity on more than 500 samples of sedimentary rocks, and derived simple relations between v_P and depth or geologic time. To keep the model simple, we drew standard velocity profiles for each geological unit using two linear slopes to reproduce the generally higher depth gradient found at shallower depth, and the gentler increase with larger depth (Figure 3). These profiles were derived by merging the curves from Faust (1951), Brocher (2008), Ogniben et al. (1975) and personal communications by R. Fantoni. Actual velocities in individual locations of the units were cut from the standard profiles, between relevant depths. Outside the basin, and below the given units, velocities were assigned according to regional seismic models (Christensen and Mooney, 1995). We completed the model scaling v_P profiles using the Brocher (2005) relations that link v_S and density to v_P.

The model

[Figure 2 about here.]

Figure 2 shows the depth of the interfaces of our new model of the Po Plain basin (that we dubbed MAMBo). The model covers the whole area of the basin, and surrounding regions — in the range 44°N – 46.5°N and 7.5°E – 14°E, with an approximately extent of 650 × 300 km— and it merges laterally into wider, and coarser, European reference crustal model EPcrust (Molinari and Morelli, 2011). MAMBo is composed by seven layers with laterally-varying thickness: shallow loose sediments; Quaternary; Pliocene; Oligo-Miocene; Paleogene; Mesozoic; and crystalline crustal units. One further layer reaches the depth of the Moho.

The model is represented by a set of objects (the interfaces define the geological units) and rules (the velocity and density gradients in each unit), implemented in a computer tool that can generate a 3D mesh with the required spacing, or local 1D profiles of seismic velocity and density at any geographical location. A working framework with a geographic spacing of 0.01° × 0.01° is used for representing the depth of interfaces. Each geological layer can taper out laterally and disappear. This framework (complemented by the rules defining velocities and density as a function of depth) can be interpolated and sampled in any 3D grid of points, as fine as the user needs to make the computational mesh. The smallest horizontal length scales represented in our framework — as can also be visually verified in the maps, see Figure 2 — are slightly less than 10 km. This scale length for instance pertains to the (perhaps most important for our purpose) base of Pliocene, it varies with geographical location, and differs for the different maps (Figure 2). Vertically, the geological bodies range in thickness from kilometres down to a hundred meters. Note that the horizontal scale length refers to the scale of variation of the interfaces defining geological bodies. Transitions between adjacent bodies are sharp, so that these discontinuities are always as sharp as the mesh that is being used — in the mesh generation needed for simulations with spectral elements (see Section 3) this corresponds to sampling the structure at the Gauss-Lobatto-Legendre quadrature points (Komatitsch and Tromp, 2002; Peter et al., 2011).

[Figure 3 about here.]

Model MAMBo inherits features from the original datasets, that reflect the main tectonic characteristics of basin. The subsurface of the Po Plain is characterized by Apennines thrust sheets and foredeep basin, resulting in a marked asymmetry in the thickness distribution of Neogene clastic sediments. These foredeep sediments thin towards the northern margin of the Po Plain, where the Mesozoic limestone units become shallower. A remarkable uplift of Mesozoic units occurs also in the Ferrara Arc, where the Mesozoic limestones are part of the thrust sheets. The ”loose sediment” unit (Figure 2a) is mapped in the central part of the basin with a thickness between a few m and 0.5 km. The P-wave velocity is fixed at 1.7 km/s. Quaternary terrains (Figure 2b) are present almost everywhere, with variable thickness ranging from ∼0.5 km in the western part of the plain to the ∼2.8km near the Adriatic coasts. P-wave velocity ranges from 1.7 km/s, in the shallower part, to 2.6 km/s in the deepest part — in agreement with Brocher (2008) and Faust (1951). The Pliocene-Quaternary sediments (Figure 2c) are as thick as 6.5-7 km near the Apennines foothills, but they thin along strike — rather abruptly — and towards the foreland — more gently (e.g. Bigi et al., 1990). The Southern Alps retro-foreland basin is mainly filled by a moderately thick succession of late Oligocene–middle Miocene sediments (Figure 2d). In the depocentral area, located in the Lombardy region (western Po Plain), the base of the succession can reach a depth of ca. 6 km (Fantoni et al., 2004; Fantoni and Franciosi, 2010a). P-wave velocity ranges from 1.8 km/s to 3.3

km/s in the Pliocene sediments — corresponding to a shear-wave velocity of $\sim$ 0.6 to 1.7 km/s via the Brocher relation (Brocher, 2005). v_P is within the range 2.4–3.8 km/s for the Oligo-Miocene lithology ($v_S \sim$ 1.0 to 2.2 km/s). The Paleogene layer is bounded by the bottom of the Oligo-Miocene lithology (Figure 2d) and the top of Mesozoic (Figure 2d-e). P-velocity (from 4.0 to 4.9 km/s) is significantly higher than in younger units due to the higher calcium-carbonate content. The top of the Mesozoic unit reflects the paleogeography of the Adriatic Tethian margin (Winterer and Bosellini, 1981; Masetti et al., 2010). The regions shallower than 2 km in the north-eastern part are related to the Friuli-Dinaric carbonate platform (east) and the Trento pelagic plateau (center); this last feature is plunging south-eastward into the Po Plain. The Friuli carbonate platform and the Trento plateau are separated by the Belluno basin, which joins southward the larger northern Adriatic basin, which was likely connected to the large Lombardy basin, that is present beneath the western part of the Po Plain (Figure 2e). A roughly north-south uplift within the Lombardy basin, where the top of the Mesozoic units is shallower than 5 km, is related to Alpine inversion of a system of Mesozoic rift basins (Fantoni et al., 2004). P-wave velocity ranges from 4.9km/s to 5.7km/s ($v_S \sim$ 2.8 to 3.4 km/s), slightly higher than the values reported by Brocher (2008). The top of the magnetic basement (Figure 2f) marks on the edge of the crystalline crust, that in our simplified model is extended to the Moho. The considerable lateral variation in seismic wave properties and the thickness of the sediments clearly appear in Figure 3c. We show seven depth-velocity profiles sampling the 3D model in the locations marked in Figure 2a. The P5 and P7 profiles, located outside the Pliocene and Oligo-Miocene deposits, show relatively thin sediment layers and high velocity crust. In fact, the Mesozoic unit starts at about two kilometers depth. The P4 (and P6), P3 and P1 profiles are located on the Quaternary, Pliocene and Oligo-Miocene depocenters respectively, and illustrate the inner structure of the basin.

Other seismic models have been proposed for this area. They are rather simplified, and they often present only one average 1D velocity profile. Vuan et al. (2011) derived a model for the Po Plain with a 1D depth-dependent velocity profile in the sedimentary filling of a basin, with a 3D shape – topography, base of Pliocene, and Moho vary laterally, in order to estimate the displacement response spectra from 3D numerical simulations. Our estimation of the P- and S-wave velocities in the consolidated sediments (Quaternary, Pliocene and Oligo-Miocene) is, on average, in agreement with their 1D-velocity profile for the Po Plain. A direct comparison, however, is not possible given the complex structure of our layers. Malagnini et al. (2012) and Milana et al. (2013) estimated average 1D models for the epicentral area of the May 2012 Ferrara seismic sequence. The former was derived from geological interpreted sections, the latter from strong motion and ambient noise data. Our velocity range at depths shallower than 6 km in this area is qualitatively in agreement with these two independent determinations.

Seismic performance

Although a detailed evaluation of the performance of model MAMBo — in terms of its ability to reproduce behaviour of the seismic wavefield at local scales — is beyond the scope of this article, we show here how it behaves in modeling seismograms recorded during two recent earthquakes. We selected two events that occurred beneath the Po Plain: the M_W=5.8 earthquake of May 29 2012, and the M_W=4.5 of 21 June 2012 (Pondrelli et al., 2012; Scognamiglio et al., 2012). The first earthquake was located in the center of the Po Plain at a depth of about 7-11 km; the second occurred in the Venetian Alps at a depth of about 9-10 km (Figure 4 and 5).

We calculated synthetic seismograms using the widely used SPECFEM3D wave propagation code (Komatitsch and Tromp, 2002; Peter et al., 2011), that implements the spectral-element method (SEM) to solve the seismic wave equation and accurately simulate complete waveforms in complex media. SEM is widely used in seismological applications to solve forward and inverse problems. In particular, it has been used to study the response of sedimentary basins (e.g. Komatitsch et al., 2004; Stupazzini et al., 2009; Tape et al., 2009) and 3D local and regional model (e.g. Magnoni et al., 2014). Of relevance for us, the SPECFEM3D code may consider finite faults and anisotropy (although we do not use such complications in the present case), besides attenuation. It allows to honor discontinuities within the model — such as basin bottoms, high resolution topography, and discontinuities related to geological bodies. The code is parallelised using a domain decomposition approach and the MPI (Message Passing Interface) standard.

We implemented the MAMBo model in the SPECFEM3D_Cartesian wave propagation code using a computational mesh of Northern Italy built with the CUBIT mesh generation package (see Data and Resources). The mesh honors the topography and the Moho depth, and it is composed of about 3 million hexahedral elements. The minimum element width of 2 km at the surface allowed us to accurately simulate seismic waves with minimum period of about 3 s. Within each element, at each of the Gauss-Lobatto-Legendre quadrature points (5 points in each direction per element) the seismic parameters were taken from the MAMBo model smoothed with a horizontal 2D Gaussian filter (σ = 6km) to avoid sharp discontinuities that could generate artefacts in the synthetic wavefield. Attenuation was scaled from shear-wave speed following Olsen et al. (2003). For comparison, we also implemented the average 1D model usually employed to locate earthquakes for the Seismic Bulletin at INGV (Figure 3c). The model consist of 2 layers over a halfspace: the first has a thickness (h) of 11.1 km and a v_P of 5.0 km/s, for the second h = 26.9 km and v_P = 6.5 km/s and the halfspace has v_P = 8.05 (for all layers v_P/v_S = 1.732).

[Figure 4 about here.]

[Figure 5 about here.]

The evaluation of MAMBo performance relies first on the ability to capture the complex shape of the data, and to reproduce such effects in synthetic waveforms calculated in our high resolution 3D model. In Figure 4 and Figure 5 we show signals recorded at selected stations inside, and around, the basin. In a relatively long period range — between 3 s and 20 s — basin resonance, amplification effects and long shaking duration appear at stations within and bordering the basin, due to the presence of thick sediments (Vuan et al., 2011; Massa and Augliera, 2013; Luzi et al., 2013). Luzi et al. (2013) observed long duration in records, generated by the May 2013 earthquake sequence, with epicentral distance larger than 30 km as a consequence of later surface wave arrivals. They noticed the presence of 5s surface waves mainly from NNE Italy to SSW. We compared such records with synthetic waveforms predicted by the MAMBo model and by the INGV Seismic Bulletin 1D model. The displacement time series were filtered between 3s and 15s, only the vertical displacement component is shown here. All traces are normalized in each window. A visual comparison between data and synthetics highlights the dramatic effects of the thick Po Plain basin on the waveforms in terms of long duration and resonance effects. Our model shows significant improvement with respect to the 1D model, that is obviously not able to account for lateral variations of the wavefield. The differences are mostly evident for propagation paths crossing the sedimentary basin where the MAMBo model reproduces the envelope of the recorded data. Overall, the arrival times of the peak ground displacement are well reproduced by the 3D model.

For the $M_W = 5.8$ earthquake inside the plain (Figure 4), we note basin-induced surface waves at stations ROTM, MONC, GUMA and PESA. The duration of shaking here is about $\sim$ 100s (or even more) and it is longer than at other stations: the wave energy travels through the whole plain, crossing the depocenter of the Pliocene deposits, that is likely the cause of these effects. The 1D model is clearly inadequate to reproduce such observations while MAMBo is able to account for these complexities: the duration of synthetics is comparable to the data as well as the arrival time of each wave packet. The signal recorded at station MONC seems to be dominated by waves with period 10-15 s, only partially modelled even by the 3D model. At the station closest to the epicenter (ZCCA), on the Apennines, the 3D model underestimates the amplitude because of a lack of detailed modeling of the structure outside the basin, while the envelope and duration are very well reproduced. We also note that at station ASQU the amplitude of shaking is well rendered by MAMBo, while at POMP it is overestimated by about a factor of 2 — note however that phase, envelope and duration are quite good. The stations to the north of the epicenter (BNALP, MABI, ROVR, STAL) show duration of the shaking of about 50s, half of the duration recorded at stations within the basin: the source-receiver paths are running mainly through crystalline rocks with only a short part through shallow Pliocene deposit. However, if we look at the signals from the 1D model, we can conclude that the plain has strong influence also on these paths, and that the 3D model is able to reproduce very well the observed wave field both in phase and envelope. The tail is well reproduced, but the maximum displacement is a little underestimated.

We note a similar behaviour for the $M_W = 4.5$ earthquake that occurred at the border between the Eastern Alps and the Po Plain. In the almost-pure rock paths (BRMO, WTTA, FVI, PTCC) waveforms are quite simple. The maximum amplitude is well fit by the 3D model, while the 1D model systematically underestimates the maximum shaking. The 3D synthetics also reproduce the envelope better than the 1D model. Signals that travel through the plain are characterized by a first part by a long wavelength, with higher-frequency waves superimposed, that are likely an effect of the complex structure beneath the plain. In some cases (MASSA, MIAM, PIEI, TEOL) MAMBo is able to reproduce such signals very well. For paths crossing the Plio-Quaternary depocenters (MSSA, MIAM) we note a long duration ($\sim$ 100s) of shaking in the data; the agreement between the envelopes of 3D synthetics and data is very good, for up to 200 s of duration. The stations at the border of the plain, such as TEOL and ROTM, are lying on a rocky outcrop surrounded by thick sediments, and show signal characterized by almost-monochromatic resonance that is only in part accommodated by the 3D synthetics. The dramatic influence of the basin on long period ground motion is also evident in the peak ground velocity maps (Figure 6). We show these maps for the two events considered. The most interesting feature, for both earthquakes, is the high correlation of ground shaking with basin shape, in particular with the Pliocene and Oligo-Miocene units. This is particularly clear for periods longer than 5 s (as shown here). Within the basin, the shaking intensity is not negligible even hundreds of kilometers away from the source, especially for the $M_W = 5.8$ earthquake (Figure 6a). The maximum amplitude we obtained in our simulation is comparable with the recorded amplitude for the periods considered Luzi et al. (2013). The peak ground velocity results quite elongated in the EW direction, in accordance with observations by Luzi et al. (2013) (Figure 7d-8d-8f). However, the NNE-SSW propagation effects result attenuated with respect to the observations. For the $M_W = 4.5$ event, of course, amplitudes are considerably lower than for the $M_W = 5.8$ event, and substantial shaking is reversed to the north-eastern part of the Po Plain basin. In both cases, the shape of shaking agrees quite well with macro-seismic intensity data (Sbarra et al,, 2010).

[Figure 6 about here.]

Discussion and conclusions

We present a 3D model of the Po Plain sedimentary basin (Italy) resulting from the assembly of extensive geological information available in the literature. The model (MAMBo) describes the main tectonic and structural features with unprecedented detail for this region. The model consists of seven 3D layers, corresponding to the main geological units, whose confining interfaces are represented in a geographical grid with a horizontal resolution of $0.01° \times 0.01°$. In each layer, v_P, v_S, and density are specified as a function of depth. The model can be re-sampled at any point on any desired mesh. It is designed for 3D numerical wave propagation calculations, and it is publicly available (see section on Data and Resources). The MAMBo basin model has been preliminarily verified through comparison between numerical simulations and recorded seismograms for two recent earthquakes. Results agree well in the low-frequency range (f <0.33 Hz – $T > 3$s). Specifically, the new model is able to reproduce the long coda, and many other features that can be observed in the data — long duration of shaking for paths crossing the basin, reflections, resonance and peak ground velocity are all well reproduced. These parameters have high relevance for engineering purposes, as as when modeling the response of high-rise buildings and soil liquefaction effects (Hancock and Bommer, 2005). The spatial distribution of maximum shaking agrees quite well with observations (Luzi et al., 2013) and with macroseismic data. This emphasizes the importance of knowledge of basin structure in 3D to predict ground shaking, since amplitude and duration are highly correlated with the basin inner structure. Our model can help to evaluate expected ground motion for plausible future earthquakes, or to predict shake maps in the immediate following of a seismic event.

We are currently limited to periods $T > 3$s, that are relevant for high-rise buildings. Further developments are needed for realistic deterministic simulations at shorter periods.

We are planning to improve the model resolution by modeling lateral variations of seismic velocities through noise-correlation tomography, and full waveform inversion. A highly detailed description of the shallow velocity structure (shallower 1-3 km), beyond even the reach of seismic tomography with the existing seismograph stations, is however needed to decrease the minimum period to $T \sim 1$ s (Kagawa et al., 2004). This includes the necessity to model the shallow 'geotechnical' layer (often modelled by the Vs30 parameter) but the sparsity of available information, confronted with the expected rapid spatial variability of the geological structure, makes the incorporation of such constraints into a large 3D models problematic (Taborda and Bielak, 2014; Flinchum et al., 2014). Stochastic synthesis is required to reach even higher frequencies — with engineering interest for low-rise residential buildings — and a hybrid deterministic-stochastic approach could be used (Mai et al., 2010). This may be a long term goal, that still needs substantial work, for which MAMBo is however a necessary starting point.

As a final note, we would like to point out that since the MAMBo model merges smoothly into wider, and coarser, European reference crustal model EPcrust (Molinari and Morelli, 2011), it can be promptly used as a constraint in travel time and surface wave inversion even in wider regions, and as a structural model for earthquake location or finite faults inversions.

Data and Resources

Model MAMBO is publicly available, and can be found at *www.bo.ingv.it/MAMBo* and/or upon request to the authors. The SPECFEM3D_Cartesian wave propagation code is available at *geodynamics.org/ cig/ software/ specfem3d.* The CUBIT mesh generation package is available at *cubit.sandia.gov.* Seismograms used in this study have been downloaded from the EIDA website – European Integrated Data Archive (*eida.rm.ingv.it*), last accessed on November, 2012. Figures have bee drawn using the Generic Mapping Tools (Wessel and Smith, 1998).

Acknowledgements

We acknowledge ENI S.p.A., and in particular, A.L. Cazzola, R. Fantoni, G. Lanfranchi and C. Cattaneo, for allowing us to work on a confidential data set. We are grateful to L. Martelli for the useful discussions and for sharing data. Careful and constructive reviews from Arthur Rogers and Associate Editor Thomas Pratt greatly improved the manuscript. This study has been partially funded by the Italian *Presidenza del Consiglio dei Ministri - Dipartimento di Protezione Civile* (DPC), through INGV-DPC Seismological Project S1, 2012-2013. This paper does not necessarily represent DPC official opinion and policy.

References

Aagaard, B. T., T. M. Brocher, D. Dolenc, D. Dreger, R. W. Graves, S. Harmsen, S. Hartzell, S. Larsen, K. McCandless, S. Nilsson, N. A. Petersson, A. Rogers, B. Sjogreen and M. L. Zoback (2008). Ground-Motion Modeling of the 1906 San Francisco Earthquake, Part II: Ground-Motion Estimates for the 1906 Earthquake and Scenario Events, *Bull. Seism. Soc. Am.* **98** 1012–1046.

Anderson, J. G., P. Bodon, J. Brune, J. Prince, S. Sing, R. Quaas and M. Onate (1986). Strong ground motion from the Michoacan, Mexico, earthquake, *Science* **233** 1043–1049.

Argnani, A. and F. Ricci Lucchi (2001). Tertiary silicoclastic turbidite systems of the northern Apennines, in *Anatomy of an Orogen: the Apennines and Adjacent Mediterranean Basins* Vai, G., Martini, I. P. E. (Editors), Springer Netherlands 327–349.

Bigi, G., D. Cosentino, M. Parotto, R. Sartori and P. Scandone (1990). Structural model of Italy 1:500.000, *CNR, Progetto Finalizzato Geodinamica*, Florence.

Bortolotti, V., P. Passerini, M. Sagri and G. Sestini (1970). The Miogeosynclinal sequences, *Sediment. Geol.* **4** 341–444.

Bragato, P., M. Sugan, P. Augliera, M. Massa and A. Vuan (2011). Moho reflection effects in the Po Plain (northern Italy) observed from instrumental and intensity data, *Bull. Seism. Soc. Am.* **101** 20142–2152.

Brocher, T. M. (2005). Empirical relations between elastic wavespeeds and density in the Earth's crust, *Bull. Seism. Soc. Am.* **95** 2081–2092.

Brocher, T. M. (2008). Compressional and shear-wave velocity versus depth relations for common rock types in Northern California, *Bull. Seism. Soc. Am.* **98** 950–968.

Burrato, P., P. Vannoli, U. Fracassi, R. Basili and G. Valensise (2012). Is blind faulting truly invisible? Tectonic-controlled drainage evolution in the epicentral area of the

May 2012, Emilia-Romagna earthquake sequence (northern Italy), *Ann. Geophys.* **55** 525–531.

Carcano, C. and A. Piccin (2002). Geologia degli acquiferi padani della Regione Lombardia, Regione Lombardia, Eni Divisione Agip, S.EL.CA. (Firenze).

Casero, P., A. Rigamonti and M. Iocca (1990). Paleogeographic relationship during Cretaceous between the northern Adriatic area and the Eastern Southern Alps, *Mem. Soc. Geol. It.* **45** 807–814.

Cassano, E., L. Anelli, R. Fichera and V. Cappelli (1986). Pianura Padana. interpretazione integrata di dati geofisici e geologici, 73 Congr. Soc. Geol. It., 29 Sett-4 Ott.

Chaljub, E., P. Moczo, S. Tsuno, P.-Y. Bard, J. Kristek, M. Käser, M. Stupazzini and M. Kristekova (2010). Quantitative comparison of four numerical predictions of 3D ground motion in the Grenoble valley, France, *Bull. Seism. Soc. Am.* **100** 1427–1455.

Christensen, N. I. and W. D. Mooney (1995). Seismic velocity structure and composition of the continental crust; a global view, *J. Geophys. Res.* **100**, 9761–9788.

Davis, J. (2002). *Statistics and Data Analysis in Geology*, 3rd Edition John Wiley & Sons.

Denolle, M. A., H. Miyake, S. Nakagawa, N. Hirata and G. C. Beroza (2014). Long-period seismic amplification in the Kanto basin from the ambient seismic field, *Geophys. Res. Lett.* **41** 2319–2325.

Devoti, R., A. Esposito, G. Pietrantonio and A. R. Pisani and F. Riguzzi (2011). Evidence of large scale deformation patterns from gps data in the italian subduction boundary, *Earth Planet. Sci. Lett.* **311** 230–241.

Dhakal, Y. D. and H. Yamanaka (2013). An evaluation of 3D velocity models of the Kanto basin for long-period ground motion simulations, *J. Seismol.* **17** 1073–1102.

Di Stefano, R., E. Kissling, C. Chiarabba, A. Amato and D. Giardini (2009). Shallow subduction beneath Italy: Three-dimensional images of the Adriatic-European-Tyrrhenian lithosphere system based on high-quality P wave arrival times, *J. Geophys. Res.* **114** B05305.

Fantoni, R., R. Bersezio and F. Forcella (2004). Alpine structure and deformation chronology at the southern Alps-Po Plain border in Lombardy, *Boll. Soc. Geol. Ital.* **123** 463–476.

Fantoni, R. and R. Franciosi (2010a). Mesozoic extension and Cenozoic compression in Po Plain and Adriatic foreland, *Rendicont. Online Soc. Geol. Ital.* **9** 28–31.

Fantoni, R. and R. Franciosi (2010b). Tectono-sedimentary setting of the Po Plain and Adriatic foreland, *Rend. Fis. Acc. Lincei* **21**(Suppl 1) S197–S209.

Faust, L. (1951). Seismic velocity as a function of depth and geologic time, *Geophysics* **16** 192–206.

Flinchum, B. A., J. N. Louie, K. D. Smith, W. H. Savran, S. K. Pullammanappallil and A. Panche (2014). Validating Nevada ShakeZoning Predictions of Las Vegas Basin Response against 1992 Little Skull Mountain Earthquake Records, *Bull. Seism. Soc. Am.* **104** 439–450.

Gebrande, H., A. Castellarin, E. Lüschen, K. Millahn, F. Neubauer and R. Nicolich (2006). TRANSALP–A transect through a young collisional orogen: Introduction, *Tectonophysics* **414** spec. 1–7.

Goto, H., S. Sawada, H. Morikawa, H. Kiku and S. Ozalaybey (2005). Modeling of 3D subsurface structure and numerical simulation of strong ground motion in the Adapazari basin during the 1999 Kocaeli earthquake, Turkey, *Bull. Seism. Soc. Am.* **95** 2197–2215.

Gualtieri, L., P. Serretti and A. Morelli (2014). Finite-difference p wave travel time seismic tomography of the crust and uppermost mantle in the Italian region, *G-cubed* **15** 69–89.

Hancock, J. and J. Bommer (2005). The effective number of cycles of earthquake ground motion, *Earthquake Engng Struct. Dyn.* **34** 637–664.

Hruby, C. E. and I. A. Beresnev (2003). Corrections for basin effects in stochastic ground-motion prediction, based on the Los Angeles Basin analysis, *Bull. Seism. Soc. Am.* **93**, 1679–1690.

Jarvis, A., H. Reuter, A. Nelson and E. Guevara (2008), Hole-filled SRTM for the globe Version 4, *available from the CGIAR-CSI SRTM 90m Database (http://srtm.csi.cgiar.org)*.

Kagawa, T., B. Zhao, K. Miyakoshi and K. Irikura (2004), Modeling of 3D basin structures for seismic wave simulations based on available information on the target area: Case study of the Osaka basin, Japan, *Bull. Seism. Soc. Am.* **94**, 1353–1368.

Kligfield, R. (1979). The northern Apennines as a collisional orogen, *Am. J. Sci.* **279** 676–691.

Koketsu, K. and M. Kikuchi (2000). Propagation of seismic ground motion in the Kanto basin, *Science* **228** 1237–1239.

Komatitsch, D., Q. Liu, J. Tromp, P. Süess, C. Stidham and J. H. Shaw (2004). Simulations of ground motion in the Los Angeles basin based upon the spectral-element method, *Bull. Seism. Soc. Am.* **94** 187–206.

Komatitsch, D. and J. Tromp (2002). Spectral-element simulations of global seismic wave propagation: I. validation, *Geophys. J. Int.* **149** 390–412.

Luzi, L., F. Pacor, G. Ameri, R. Puglia, P. Burrato, M. Massa, P. Augliera and R. Castro (2012). Overview on the strong motion data recorded during the May-June 2012 Emilia seismic sequence, *Seismol. Res. Lett.* **84** 629–644.

Magistrale, H., K. McLaughlin and S. M. Day (1996). A geology-based 3D velocity model of the Los Angeles Basin sediment, *Bull. Seism. Soc. Am.* **86** 1161–1166.

Magistrale, H., S. M. Day, R. W. Clayton and R. Graves (2000). The SCEC Southern California reference three-dimensional seismic velocity model Version 2, *Bull. Seism. Soc. Am.* **90**, S65–S76.

Magnoni, F., E. Casarotti, A. Michelini, A. Piersanti, D. Komatitsch, D. Peter and J. Tromp (2014). Spectral-element simulations of seismic waves generated by the 2009 l'Aquila earthquake, *Bull. Seism. Soc. Am.* **104** 1–22.

Mai, P. M., W. Imperatori and K. B. Olsen (2010). Hybrid broadband ground-motion simulations: Combining long-period deterministic synthetics with high-frequency multiple s-to-s backscattering, *Bull. Seism. Soc. Am.* **100** 2124– 2142.

Malagnini, L., R. B. Herrmann, I. Munafò, M. Buttinelli, M. Anselmi, A. Akinci and E. Boschi (2012). The 2012 Ferrara seismic sequence: Regional crustal structure, earthquake sources, and seismic hazard, *Geophys. Res. Lett.* **39**, –.

Masetti, D., R. Fantoni, R. Romano, D. Sartorio and E. Trevisani (2010). Tectonostratigraphic evolution of the Jurassic extensional basins of the eastern southern Alps and Adriatic foreland based on an integrated study of surface and subsurface data, *AAPG Bull.* **96** 2065–2089.

Massa, M. and P. Augliera (2013). Teleseisms as estimators of experimental long-period site amplification: Application to the Po plain (Italy) for the 2011 M_w 9.0 Tohoku-Oki (Japan) earthquake, *Bull. Seism. Soc. Am.* **103** 2541–2556.

Massa, M., P. Augliera, G. Franceschina, S. Lovati, and M. Zupo (2012). The July 17, 2011, ML 4.7 Po Plain (northern Italy) earthquake: strong-motion observations from the RAIS network. *Ann. Geophys.* **55** 309–321.

McPhee, D. K., V. E. Langenheim, S. Hartzell, R. J. McLaughlin, B. T. Aagaard, R. C. Jachens, and C. McCabe (2007). Basin Structure beneath the Santa Rosa Plain, Northern California: Implications for Damage Caused by the 1969 Santa Rosa and 1906 San Francisco Earthquakes, *Bull. Seism. Soc. Am.* **97** 1449-1457.

Meletti, C., V. D'Amico, G. Ameri, A. Rovida and M. Stucchi (2012). Seismic hazard in the Po Plain and the 2012 Emilia earthquakes, *Ann. Geophys.* **55** 623–629.

Milana, G., P. Bordoni, F. Cara, G. Giulio, S. Hailemikael and A. Rovelli (2013). 1D velocity structure of the Po River plain (Northern Italy) assessed by combining strong motion and ambient noise data, *Bull. Earthquake Eng.* **12** 2195–2209.

Molinari, I. and A. Morelli (2011). EPcrust: A reference crustal model for the european plate, *Geophys. J. Int.* **185** 352–364.

Molinari, I., V. Raileanu and A. Morelli (2012). A crustal model for the Eastern Alps region and a new Moho map in South-Eastern Europe, *Pure Appl. Geophys.* **169** 1575–1588.

Nicolich, R., B. Della Vedova, M. Giustinani and R. Fantoni (2004). Carta del sottosuolo della pianura friulana, *Regione Autonoma Friuli Venezia-Giulia, Direzione Centrale Ambiente e Lavori pubblici, Servizio Geologico.*

Ogniben, L., M. Parotto and A. Praturlon (1975). Structural model of Italy. *Quaderni de "La ricerca scientifica"*, Progetto finalizzato Geodinamica: Risultati finali. Consiglio Nazionale delle Ricerche, Roma **114**-3.

Olsen, K. B. (2000). Site amplification in the Los Angeles basin from three-dimensional modeling of ground motion, *Bull. Seism. Soc. Am.* **90** S77–S94.

Olsen, K. B., S. M. Day and C. R. Bradley (2003). Estimation of q for long- period (¿2 sec) waves in the Los Angeles basin, *Bull. Seism. Soc. Am.* **93** 627–638.

Patacca, E., R. Sartori and P. Scandone (1992). Tyrrhenian basin and Apenninic arcs. Kinematic relations since late Tortonian times, *Memor. Soc. Geol. Ital.* **45** 425–451.

Peter, D., D. Komatitsch, Y. Luo, R. Martin, N. L. Goff, E. Casarotti, P. L. Loher, F. Magnoni, Q. Liu, C. Blitz, T. Nissen-Meyer, P. Basini and J. Tromp (2011). Forward and adjoint simulations of seismic wave propagation on fully unstructured hexahedral meshes, *Geophys. J. Int.* **186** 712–739.

Piana Agostinetti, N. and A. Amato, (2009). Moho depth and Vp/Vs ratio in peninsular Italy from teleseismic receiver functions, *J. Geophys. Res.* **114** B06303.

Pieri, M. and Groppi, (1981). Subsurface geological structures of the Po Plain. *CNR, Progetto Finalizzato Geodinamica* 414.

Pondrelli, S., S. Salimbeni, P. Perfetti and P. Danecek (2012). Quick regional centroid moment tensor solutions for the Emilia 2012 (northern Italy) seismic sequence, *Ann. Geophys.* **55** 615–621.

RER, ENI-Agip (1998). Riserve idriche sotterranee della Regione Emilia-Romagna, *Publication Regione Emilia Romagna.*

Roten, D., Fäh, D., K. B. Olsen and D. Giardini (2008). A comparison of observed and simulated site response in the Rhône valley, *Geophys. J. Int.* **173** 958–978.

Scognamiglio, L., L. Margheriti, F. M. Mele, E. Tinti, A. Bono, P. De Gori, V. Lauciani, F. P. Lucente, A. G. Mandiello, C. Marcocci, S. Mazza, S. Pintore and M. Quintiliani (2012). The 2012 Pianura Padana emiliana seimic sequence: locations, moment tensors and magnitudes, *Ann. Geophys.* **55** 549–559.

Scrocca, D., C. Doglioni, F. Innocenti, P. Manetti, A. Mazzotti, L. Bertelli, L. Burbi and S. D'Offizi (2003). Crop atlas: seismic reflection profiles of the italian crust, *Mem. Descr. Carta Geol. It.* **61** 1–194.

Sbarra, P., P. Tosi and V. De Rubeis (2010). Web based macroseismic survey in Italy: method validation and results, *Nat. Hazards* **54** 563-581.

Spada, M., I. Bianchi, E. Kissling, N. P. Agostinetti and S. Wiemer (2013). Combining controlled-source seismology and receiver function information to derive 3-D Moho topography for Italy, *Geophys. J. Int.* **194** 1050–1068.

Speranza, F. and M. Chiappini (2002). Thick-skinned tectonics in the external Apennines, Italy: New evidence from magnetic anomaly analysis, *J. Geoph. Res.* **107** ETG 8-1–ETG 8-19.

Stehly, L., B. Fry, M. Campillo, N. M. Shapiro, J. Guilbert, L. Boschi and D. Giardini

(2009). Tomography of the Alpine region from observations of seismic ambient noise, *Geophys. J. Int.* **178** 338–350.

Stupazzini, M., R. Paolucci and H. Igel, 2009. Near-fault earthquake ground-motion simulation in the Grenoble valley by a high-performance spectral element code, *Bull. Seism. Soc. Am.* **99** 286–301.

Süss, M. P. and J. H. Shaw (2003). P wave seismic velocity structure derived from sonic logs and industry reflection data in the Los Angeles basin, California, *J. Geophys. Res.* **108**.

Taborda, R. and J. Bielak (2014). Ground-Motion Simulation and Validation of the 2008 Chino Hills, California, Earthquake Using Different Velocity Models, *Bull. Seism. Soc. Am.* **104** 1876–1898.

Tape, C., Q. Liu, A. Maggi and J. Tromp (2009). Adjoint tomography of the Southern California crust, *Science* **325** 988–9922.

Vuan, A., P. Klin, G. Laurenzano and E. Priolo (2011). Far-source long-period displacement response spectra in the Po and Venetian Plains (Italy) from 3D wavefield simulations, *Bull. Seism. Soc. Am.* **101** 1055–1072.

Wessel, P. and W. H. F. Smith (1998). New, improved version of the Generic Mapping Tools released, *Eos Trans. AGU* **79** 579.

Winterer, E. L. and A. Bosellini (1981). Subsidence and sedimentation on Jurassic passive continental margin, southern Alps, Italy, *AAPG Bulletin* **65** 394–421.

List of Figures

1 Coverage of datasets used in construction of the surface grids. 28

2 Depth of the discontinuity surfaces within the MAMBo model. a) Base of "loose sediment"; b) base of Quaternary; c) Base of Pliocene; d) base of Oligo-Miocene; e) top of Mesozoic, in which we label LB=Lombardy Basin, LI=Lacchiarella Alpine Inversion, TP=Trento Plateau, NAB=Northern Adriatic Basin, BB=Belluno Basin, FDP=Friuli-Dinaric Platform; f) top of magnetic basement. 29

3 a) Schematic cartoon illustrating the lithological units identified in this work. b) P-wave velocity profiles associated with each layer (left) and S-wave velocity profiles (right) scaled from v_P via Brocher's relations (Brocher, 2005) ; c) depth-velocity (and density) profiles extracted from the 3D model at the points (P1-7) reported in Figure 2a showing the lateral variation in seismic wave properties. In each panel, the dotted line represents v_P (km/s) of the 1D model used for the simulations (see text). 30

4 Displacement waveform comparison for the May 29, 2012, $M_W = 5.8$ event. The epicentre is marked by the focal mechanism used in the simulation in the map in the center panel, also showing stations (triangles) and depth to bottom of Pliocene, perhaps one of the most significant discontinuity representing sedimentary thickness (km) for wave propagation purposes. Middle traces are vertical component of recorded seismograms filtered between 3s and 15s, bottom traces are synthetics computed with the 1D model, and top traces are synthetics computed in the MAMBo 3D model. Amplitudes are normalised for each panel and maximum amplitudes are annotated. . 31

5 Same as Figure 4 for the June 21, 2012, $M_W = 4.5$ event. 32

6 Peak ground velocity (cm/s) predicted by the 3D MAMBo model for period T> 5s for a) $M_W = 5.8$ earthquake occurred on 29 May 2012 (maximum of 6.96cm/s) and b) $M_W = 4.5$ earthquake on 09 June 2012 (maximum of 0.0059cm/s). The dashed line follows the Po Plain boundaries at the surface. 33

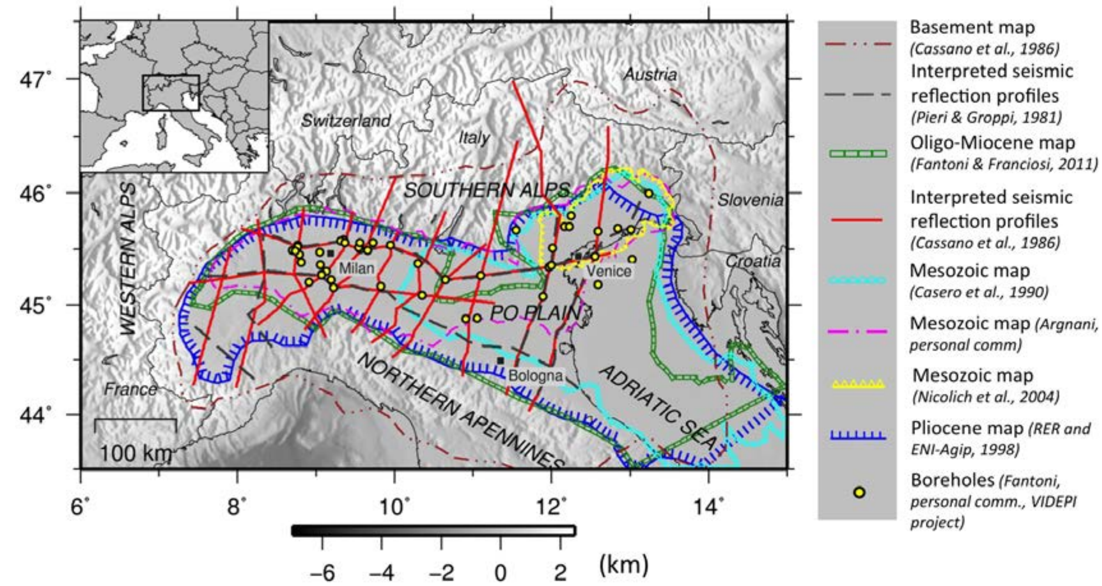

Figure 1: Coverage of datasets used in construction of the surface grids.

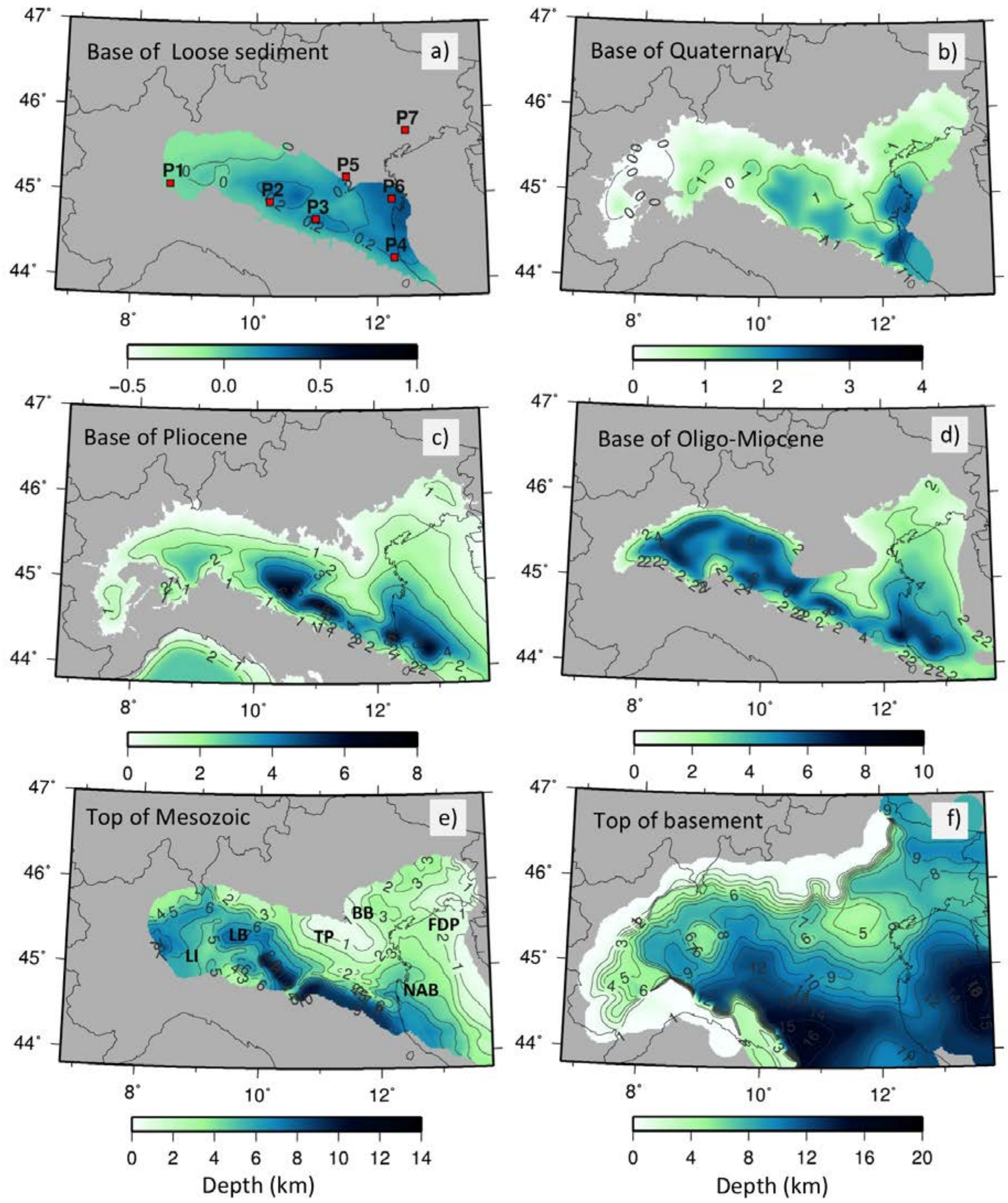

Figure 2: Depth of the discontinuity surfaces within the MAMBo model. a) Base of "loose sediment"; b) base of Quaternary; c) Base of Pliocene; d) base of Oligo-Miocene; e) top of Mesozoic, in which we label LB=Lombardy Basin, LI=Lacchiarella Alpine Inversion, TP=Trento Plateau, NAB=Northern Adriatic Basin, BB=Belluno Basin, FDP=Friuli-Dinaric Platform; f) top of magnetic basement.

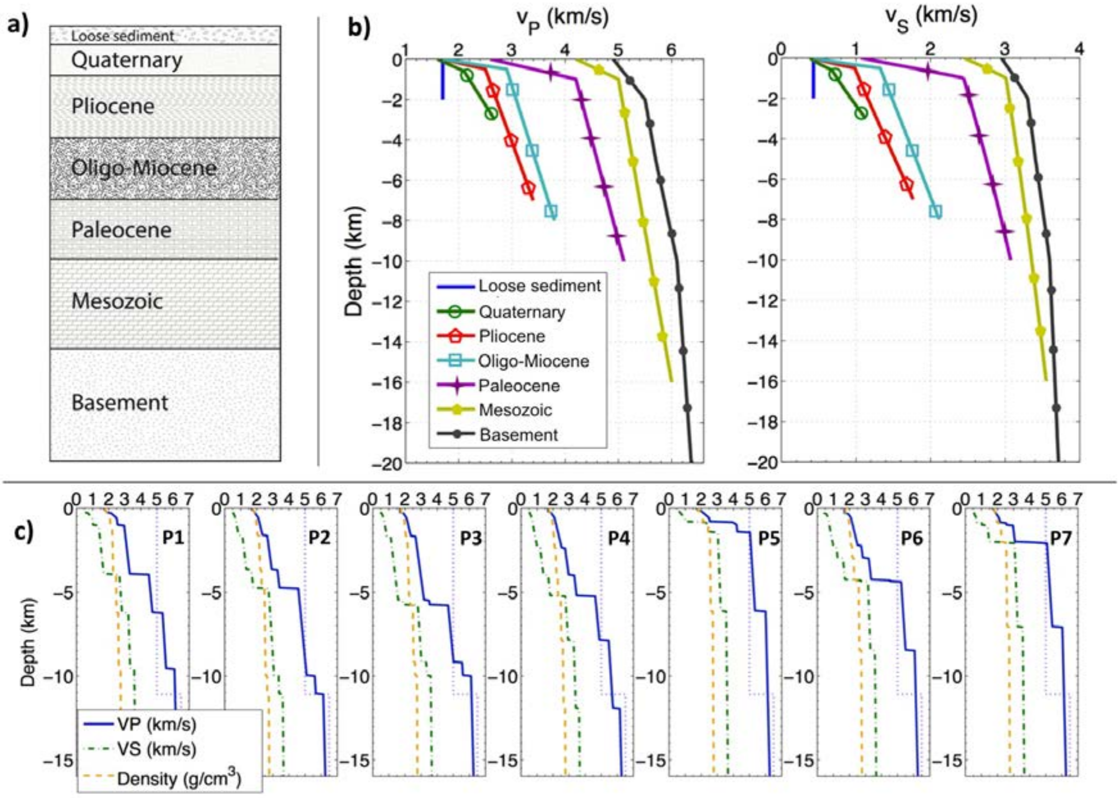

Figure 3: a) Schematic cartoon illustrating the lithological units identified in this work. b) P-wave velocity profiles associated with each layer (left) and S-wave velocity profiles (right) scaled from v_P via Brocher's relations (Brocher, 2005) ; c) depth-velocity (and density) profiles extracted from the 3D model at the points (P1-7) reported in Figure 2a showing the lateral variation in seismic wave properties. In each panel, the dotted line represents v_P (km/s) of the 1D model used for the simulations (see text).

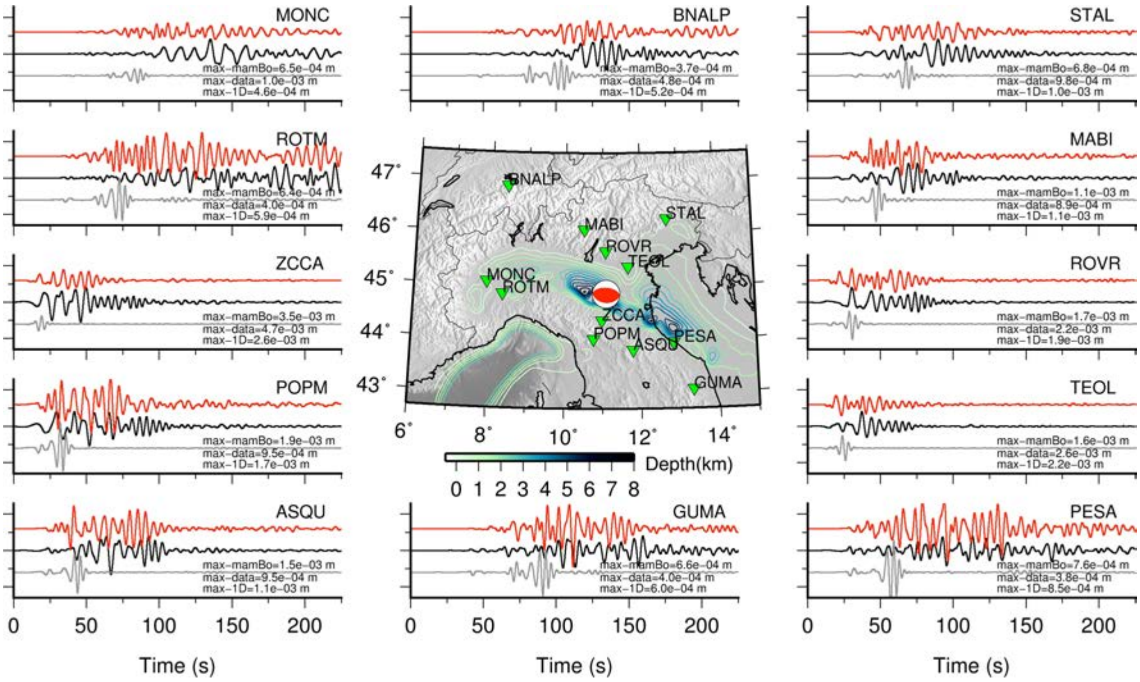

Figure 4: Displacement waveform comparison for the May 29, 2012, $M_W = 5.8$ event. The epicentre is marked by the focal mechanism used in the simulation in the map in the center panel, also showing stations (triangles) and depth to bottom of Pliocene, perhaps one of the most significant discontinuity representing sedimentary thickness (km) for wave propagation purposes. Middle traces are vertical component of recorded seismograms filtered between 3s and 15s, bottom traces are synthetics computed with the 1D model, and top traces are synthetics computed in the MAMBo 3D model. Amplitudes are normalised for each panel and maximum amplitudes are annotated.

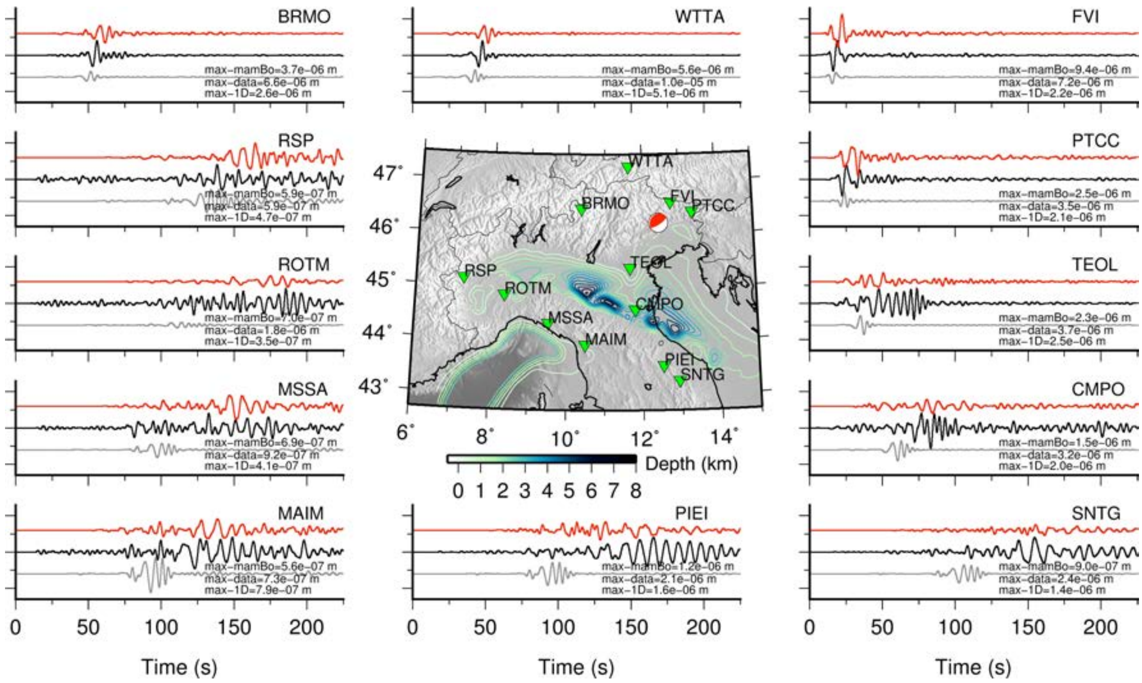

Figure 5: Same as Figure 4 for the June 21, 2012, $M_W = 4.5$ event.

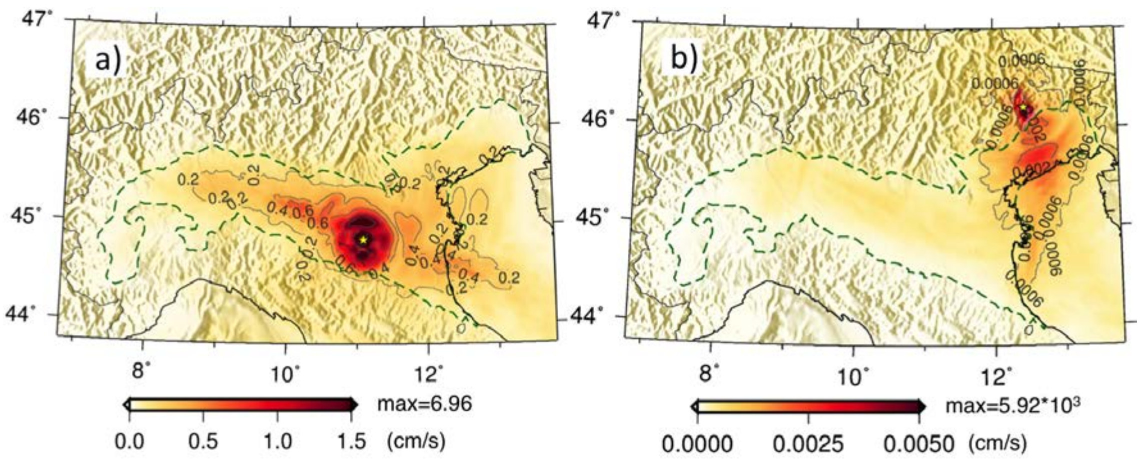

Figure 6: Peak ground velocity (cm/s) predicted by the 3D MAMBo model for period T> 5s for a) $M_W = 5.8$ earthquake occurred on 29 May 2012 (maximum of $6.96 cm/s$) and b) $M_W = 4.5$ earthquake on 09 June 2012 (maximum of $0.0059 cm/s$). The dashed line follows the Po Plain boundaries at the surface.